ACS APPLIED MATERIALS & INTERFACES

www.acsami.org

Research Article

# Electro-Optic Modulation Using Metal-Free Perovskites

Yuan Gao, Shadi Meshkat, Andrew Johnston, Chao Zheng, Grant Walters, Qixin Feng, Xiaoping Wang, Meng-Jia Sun, Amin Morteza Najarian, Dingjiang Xue, Ya-Kun Wang, Makhsud I. Saidaminov, Oleksandr Voznyy, Sjoerd Hoogland, and Edward H. Sargent*

Cite This: https://doi.org/10.1021/acsami.1c03406

Read Online

ACCESS | Metrics & More | Article Recommendations | Supporting Information

**ABSTRACT:** Electro-optic (EO) modulation is of interest to impart information onto an optical carrier. Inorganic crystals—most notably $LiNbO_3$ and $BaTiO_3$—exhibit EO modulation and good stability, but are difficult to integrate with silicon photonic technology. Solution-processed organic EO materials are readily integrated but suffer from thermal degradation at the temperatures required in operating conditions for accelerated reliability studies. Hybrid organic−inorganic metal halide perovskites have the potential to overcome these limitations; however, these have so far relied on heavy metals such as lead and cadmium. Here, we report linear EO modulation using metal-free perovskites, which maintain the crystalline features of the inorganic EO materials and incorporate the flexible functionality of organic EO chromophores. We find that, by introducing a deficiency of cations, we reduce the symmetry in the perovskite crystal and produce thereby an increased EO response. The best-engineered perovskites reported herein showcase an EO coefficient of 14 pm $V^{-1}$ at a modulation frequency of 80 kHz, an order of magnitude higher than in the nondefective materials. We observe split peaks in the X-ray diffraction and neutron diffraction patterns of the defective sample, indicating that the crystalline structure has been distorted and the symmetry reduced. Density functional theory (DFT) studies link this decreased symmetry to $NH_4^+$ deficiencies. This demonstration of EO from metal-free perovskites highlights their potential in next-generation optical information transmission.

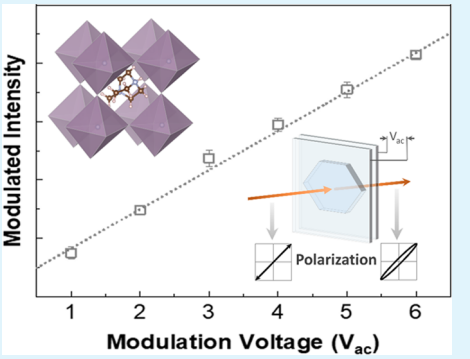


**KEYWORDS:** *electro-optic modulation, perovskite, nonlinear optic, Pockels effect, metal-free perovskite*



## 1. INTRODUCTION

Devices that efficiently convert electric signals to optical signals, electro-optic (EO) modulators, are used in optical communication. To be integrated within silicon photonic circuits, EO modulators should be compatible with the operating voltages used in CMOS; have a large modulation bandwidth as well as low optical loss and a high extinction ratio; be stable at the high operating temperatures; and be compatible with on-chip integration.[1] Attractively, silicon-based EO modulators lever silicon manufacturing processes; however, the lack of Pockels effect in silicon, and the consequent reliance on the plasma dispersion effect for phase modulation, leads to long device lengths and a significant insertion loss due to free carrier absorption.[2]

Today, lithium niobate ($LNbO_3$, also abbreviated LN) is used for EO modulation in off-chip applications, and LN modulators have seen further progress and wider deployment in recent years.[3] In an LN modulator, light is modulated via the linear EO (Pockels) effect. The recent emergence of LN-on-insulator configurations has improved the optical loss, switching voltage, and bandwidth of LN modulators.[4,5] State-of-the-art LN modulators possess a high operating bandwidth (70 Gbit $s^{-1}$) and a low optical loss (<0.5 dB) at a CMOS-compatible voltage (1.4 V).[1] However, due to the difficulties of etching LN and costly substrate integration processes,[3,6] LN modulator technology is not yet widely integrated on silicon photonics chips.

Organic polymers are solution-processed and can be integrated with silicon photonics, and have been investigated for EO modulation.[7−11] Electronic delocalization in many organic polymers results in excellent EO behavior at the molecular scale.[12] To enable efficient devices, one must arrange the EO chromophores such that the symmetry requirements for linear EO modulation are satisfied. Applying a poling field while heating the molecules above the glass transition temperature of the hosting polymer induces alignment of the dipoles, which is frozen in the aligned state upon cooling of the material.[12] Unfortunately, the orientation is unstable, and the molecules decay back to the random state that lacks EO performance.[12] In addition to thermal stability, EO chromophores with large dipole moments tend to

Received: February 21, 2021
Accepted: March 31, 2021

aggregate and be resistant to poling altogether, which limits the macroscopic EO performance.[13]

Metal halide perovskites ($ABX_3$) are solution-processed and enable templated growth,[14] allowing for potential integration with photonic chips. Some feature a noncentrosymmetric crystal structure; however, so far, their linear EO response has been less than or equal to 2 pm $V^{-1}$, the result of low spontaneous polarization.[15]

We focused instead on EO modulation using metal-free perovskites: we sought to combine the benefits of organic (processability) and inorganic (robustness) EO media. The metal-free perovskite [methyl-1,4-diazabicyclo[2.2.2]octane ammonium iodide $(MDABCO)NH_4I_3$] is known to have an impressively high spontaneous polarization (22 $\mu C\ cm^{-2}$) compared to other halide perovskites (typically below 10 $\mu C\ cm^{-2}$).[16] Since the linear EO coefficient is proportional to the spontaneous polarization,[17] we expected a larger EO response from $(MDABCO)NH_4I_3$ crystals. These metal-free perovskites are solution-processed at low temperatures (100 °C), facilitating on-chip integration. This is the first report of linear EO response that works at a high modulation frequency in metal-free perovskites.

## 2. EXPERIMENTAL SECTION

**2.1. Crystal Growth.** 1-Methyl-1,4-diazabicyclo[2.2.2]octanium iodide (MDABCOI) was prepared via the Menshutkin reaction. One gram of diazabicyclo[2.2.2]octane (DABCO) was dissolved in 30 mL of acetone at room temperature with mechanical stirring. Typically, 0.55 mL of iodomethane in 10 mL was added to the flask dropwise. The white solid was separated from the solution with centrifugation and washed with methanol and diethyl ether, and dried in vacuum. Two hundred fifty-four milligrams of MDABCOI, 145 mg of ammonium iodide, 2 mL of hydroiodic acid (57 wt % in water), 0.4 mL of hypophosphorous acid (50 wt % in water), and 0.5 mL of water were mixed in a vial. For the deficient sample, 130 mg of ammonium iodide was added. The vial was placed in a Muffle furnace, and the temperature was decreased from 100 °C to room temperature over the course of 3 days.

**2.2. Neutron Scattering.** Time-of-flight single-crystal neutron diffraction (SCND) was performed on the TOPAZ diffractometer at the Spallation Neutron Source (Oak Ridge National Laboratory).[18] The crystal was mounted on a MiTeGen loop using a small amount of Super Glue. The crystal was measured for approximately 36 h at 295 K using 20 sample orientations with 5e12C of proton charge each. The data collection strategy was obtained with CrystalPlan software.[19] The completeness of coverage of reflections in the reciprocal space was optimized using the orientation matrix obtained from the initial sample centering. Peak integration and data reduction were performed in accordance with previously reported procedures.[20] The reduced unmerged data were saved in SHELX HKLF2 format, in which the wavelength was recorded separately for each reflection.[21]

## 3. RESULTS AND DISCUSSION

We began by growing $(MDABCO)NH_4I_3$ crystals using a slow-cooling method. The crystals are transparent and have a hexagonal shape (Supporting Information, Figure S1). Samples exhibited second harmonic generation (SHG), something we account for through the anharmonic motion of the electrons, and consistent with a noncentrosymmetric crystalline structure (Supporting Information, Figure S2). Single-crystal X-ray diffraction (XRD) was used to identify the crystalline structure: we found that the $(MDABCO)NH_4I_3$ crystals possess a noncentrosymmetric space group $R3$ (Figure 1). The $(MDABCO)NH_4I_3$ crystal exhibits a direct band gap (as suggested by the calculated bandstructure, see the Supporting Information, Figure S3). The refractive index of the crystal was determined using ellipsometry. The imaginary part ($\kappa$) of the refractive index characterizes the optical absorption of the crystal and shows an absorption onset at 5.25 eV (Supporting Information Figure S4). The band gap is in the mid-ultraviolet (mid-UV) spectral range, making the crystal of potential interest for EO applications in the visible and infrared telecommunication wavelengths (such as 1.3 and 1.55 $\mu$m) since it is substantially transparent in these spectral regimes.

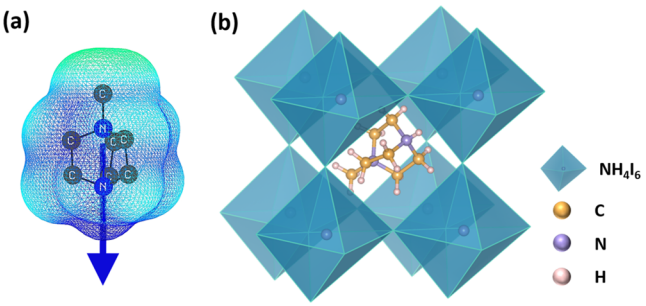


**Figure 1.** Alignment of polar molecules in metal-free perovskite. (a) Molecular structure and dipole moment of MDABCO and (b) the crystal structure of $(MDABCO)NH_4I_3$ crystals.

The methyl group on $MDABCO^{2+}$ breaks the centrosymmetry of $DABCO^{2+}$, inducing a dipole moment along the 3-fold rotation axis (Figure 1a). The $MDABCO^{2+}$ cation possesses a dipole moment of 1.69 Debye. As seen in Figure 1b, the $MDABCO^{2+}$ cations are aligned with the methyl group, pointing along the [111] axis. As a result, the molecular dipoles constructively combine to enable spontaneous polarization along the unit cell body diagonal. The perovskite framework acts as a scaffold to achieve this alignment, and, as a result, electrical poling is not needed to align the dipoles.

As in conventional inorganic ferroelectric perovskites such as barium titanate, the collective off-center displacement of the ammonium cations along the [111] direction (single-crystal X-ray diffraction, Figure 1b), also contribute to overall spontaneous polarization in the crystal.[16] Within the $NH_4I_6$ octahedra, the charge transfer enabled by hydrogen bonding between the ammonium and iodide contributes to spontaneous polarization and breaking of the crystalline centrosymmetry.[16] Taken together, the ordering of MDABCO cations, off-center displacement of ammonium cations, and charge transfer through hydrogen bonds enable a large spontaneous polarization in the $(MDABCO)NH_4I_3$ crystals.[16] Considering the linear relation between polarization and EO response,[17] we, therefore, predict a large linear EO response from the metal-free crystals.

Since the linear EO response is proportional to the spontaneous polarization of the crystal, understanding the direction and magnitude of the polarization will assist in the EO performance characterization. In crystals, the charge wave function distribution is typically delocalized and spatially continuous, and a Berry phase polarization best characterizes the overall polarization. The polarization difference, $\Delta P$, between the centrosymmetric (above Curie temperature of the crystal) and noncentrosymmetric (below the Curie temperature) phase is a Berry phase, which includes both the electronic and ionic contribution from the crystal.

We therefore used the Berry phase method to investigate the spontaneous polarization in the $(MDABCO)NH_4I_3$ crystals. The calculated dipole moment across eight unit cells has


https://doi.org/10.1021/acsami.1c03406
ACS Appl. Mater. Interfaces XXXX, XXX, XXX−XXX

roughly equal components along the *a*, *b*, and *c* axes (i.e., 23.1, 22.6, 20.1 Debye). As a result, the overall polarization is approximately along the body diagonal (only 3.4° off of the body diagonal) of the crystal unit cell and has a value of 4.31 $\mu$C cm$^{-2}$: the EO measurements we report in this work were done along the body diagonal.

Because the crystal is of the space group *R*3, the linear EO coefficient tensor of the crystal can be written:[22]

$$\begin{bmatrix} r_{11} & -r_{22} & r_{13} \\ -r_{11} & r_{22} & r_{13} \\ 0 & 0 & r_{33} \\ r_{41} & r_{51} & 0 \\ r_{51} & -r_{41} & 0 \\ -r_{22} & -r_{11} & 0 \end{bmatrix} \quad (1)$$

We employed density functional theory (DFT) to calculate the linear and nonlinear electronic susceptibilities of crystals of (MDABCO)$NH_4I_3$, seeking better to understand the linear EO effect better and determine the relation among tensor elements. The optical dielectric constants ($\varepsilon_{ij}^{\infty}(\omega)$) and nonlinear susceptibility for a static modulation field (nonlinear LEO susceptibility, $\chi_{ijk}^{(2)}(-\omega; \omega, 0)$) are provided in Table 1 for the stoichiometric crystal. From these values, we also derived the electronic contributions to the linear EO coefficients $r_{13}$ and $r_{33}$ (Table 2).

**Table 1. Optical Linear and Nonlinear Electronic Susceptibilities Obtained Using DFPT Calculations**

| optical dielectric constant, $\varepsilon_{ij}^{\infty}(\omega)$ | | nonlinear susceptibility, $\chi_{ijk}^{(2)}(-\omega; \omega, 0)$ [pm V$^{-1}$] | |
|---|---|---|---|
| $\varepsilon_{11}$ | 3.113 | $\chi_{113}^{(2)}$ | 0.9103 |
| $\varepsilon_{22}$ | 3.113 | $\chi_{223}^{(2)}$ | 0.9103 |
| $\varepsilon_{33}$ | 3.069 | $\chi_{333}^{(2)}$ | 1.945 |

**Table 2. Components of the Linear Electro-Optic Coefficient Tensor (Electronic Contributions) Obtained Using DFPT Calculations**

| electro-optic tensor element | pm V$^{-1}$ |
|---|---|
| $r_{13}$ | 0.188 |
| $r_{33}$ | 0.413 |

To characterize the linear EO effect, we used the Teng–Man method in transmission mode (Figure 2a). The wavelength of the laser used was 1.55 $\mu$m, one relevant to optical networking.[23] The incident laser was linearly polarized at an angle of 45° with respect to the incident plane, which results in equal magnitude s- (parallel) and p- (perpendicular) polarized light. The difference in the phase change can be written as

$$\varphi_{sp} = \frac{2\pi d}{\lambda}\left(\sqrt{n_o^2 - \sin^2\theta} - \frac{n_o}{n_e}\sqrt{n_e^2 - \sin^2\theta}\right) \quad (2)$$

where *d* is the thickness of the crystal, $\lambda$ is the laser wavelength, $\theta$ is the angle of incidence, and $n_o$ and $n_e$ are the ordinary and extraordinary refractive index, respectively.

In our setup, we use a Soleil–Babinet compensator to tune the phase retardation $\varphi_{sp}$ between the s- and p-component. After the phase compensator, the laser passes through an analyzer, which is set at a right angle to the polarizer. The signal is detected using a Ge detector.

The [111] axis of the crystals with a hexagonal shape is normal to the top surface.[16] The orientation of the crystal was confirmed via X-ray diffraction. To apply an electric field along the direction of the polarization, we use indium tin oxide (ITO)-coated glass (60 nm $Al_2O_3$ insulating layers were deposited on the surface ITO layer to prevent the current flow through the crystals). When the electric field is applied along the *z*-axis (the axis of symmetry), the index ellipsoid can be reduced to

$$\left(\frac{1}{n_o^2} + r_{13}E_z\right)(x^2 + y^2) + \left(\frac{1}{n_e^2} + r_{33}E_z\right)z^2 = 1 \quad (3)$$

In transmission differential ellipsometry, the electric-field-induced variation in the ellipticity of the transmitted laser is recorded. To improve sensitivity, an AC voltage ($V_{ac}$) is applied across the crystal, and the output from the detector is analyzed by a lock-in amplifier. When $\varphi_{sp}$ is equal to $\pi/2$:

$$\frac{I_{ac}}{I_c} \approx \delta\varphi_{sp} \quad (4)$$

$$r_{33} = \frac{\lambda}{\pi}\frac{I_{ac}}{I_c V_{ac}} \left[\frac{n_o n_e \sin^2\theta}{\sqrt{n_e^2 - \sin^2\theta}} + \frac{r_{13}}{r_{33}}\left(\frac{n_o^3}{n_e}\sqrt{n_e^2 - \sin^2\theta} - \frac{n_o^4}{\sqrt{n_o^2 - \sin^2\theta}}\right)\right]^{-1} \quad (5)$$

where $I_{ac}$ and $I_c$ are the field-induced variation of the transmitted power and the power of the transmitted laser, respectively. As shown in Figure 2b, the modulated power $I_{ac}$ increases linearly with the applied AC voltage. The linear relationship between $I_{ac}$ and $V_{ac}$ confirms a linear EO response from the crystal and excludes the third-order optical nonlinearity (Kerr effect), i.e., a rise in modulated power that grows quadratically with V. Linear modulation is a crucial aspect of optical modulation in an analogue system[24] and in advanced digital data transmission systems (such as quadrature amplitude modulation). The EO coefficient of the metal-free perovskite is 1.2 pm V$^{-1}$. To increase the EO response, we need to increase the polarization and the degree of noncentrosymmetry of crystals.

Seeking to reduce further the symmetry of the crystal, we investigated lattice distortion into the crystal. We postulated that we could introduce lattice distortions by making nonstoichiometric perovskite materials with $NH_4^+$ deficiencies. To verify this experimentally, we reduced the amount of $NH_4^+$ during crystal growth. The powder X-ray diffraction (XRD) measurements confirmed the lattice distortions with the split diffraction peaks (Figure 3b), which was predicted with DFT to be a signature of the lattice distortions (Figure 3a). We measured single-crystal neutron diffraction of large crystals of both the deficient and reference perovskites: the neutron diffraction peaks of the deficient sample also show splitting (Figure 3c), consistent with the X-ray diffraction results. The neutron diffraction was carried out on a macroscopic crystal (~5.0 × 5.0 × 2.0 mm$^3$) to ensure that the increased lattice distortion was present throughout the entire crystal rather than on a microscopic scale.


https://doi.org/10.1021/acsami.1c03406
ACS Appl. Mater. Interfaces XXXX, XXX, XXX−XXX

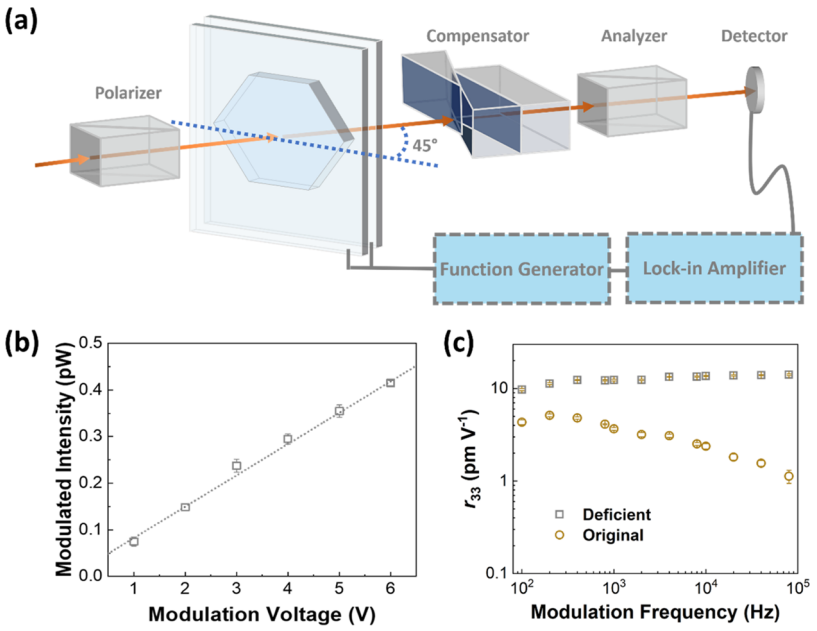


**Figure 2.** EO characterization using ellipsometry. (a) Ellipsometry setup (Teng–Men method) for the measurements of the EO coefficients. (b) Linear relationship between the modulated transmitted intensity and the modulation voltage, which confirms the linear EO effect. (c) EO coefficient as a function of modulation frequency for the original and deficient (MDABCO)$NH_4I_3$ crystals.

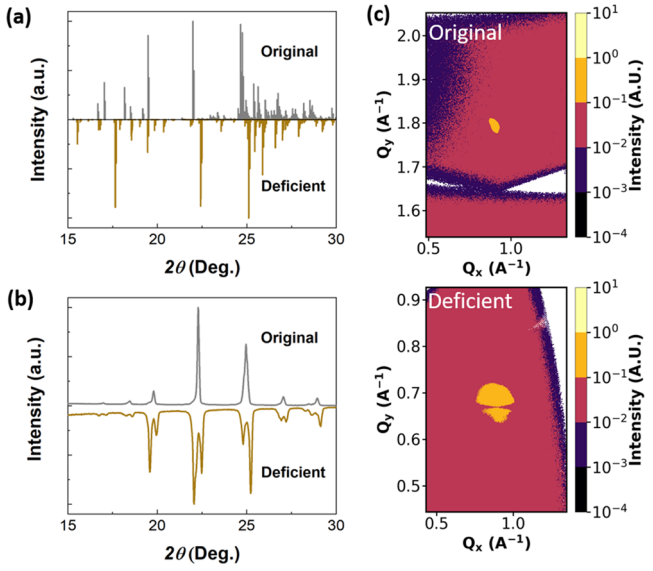


**Figure 3.** Crystal-structural characterization. (a) DFT-simulated powder XRD pattern. (b) Powder XRD pattern of original (MDABCO)$NH_4I_3$ crystals that do not contain deficiencies and deficient crystals. (c) Neutron scattering pattern of the original and deficient MDABCO–$NH_4$–$I_3$ crystals.

We measured the EO response of the original and the deficient sample from low to high frequency (80 kHz, limited by the bandwidth of the lock-in amplifier, Figure 2c; future studies are needed of high-frequency characterization based on on-chip modulators with perovskite as active material.). We found that the cation-deficient crystal exhibits a linear EO coefficient ($r_{33}$) of 14 pm V$^{-1}$ at 80 kHz. In contrast, the control sample exhibited an $r_{33}$ of 1.2 pm V$^{-1}$, a full order of magnitude lower than the deficient sample. We associate the increased EO response with the reduced symmetry of the deficient crystals. The total coefficient experimentally measured at low modulation frequencies is 10 times the calculated electronic contribution to $r_{33}$ (Table 2), indicating that a significant portion of the overall EO effect arises from the polarization of the atoms in the crystal.

We also measured the stability of the (MDABCO)$NH_4I_3$ crystals. In contrast with previously reported organic EO polymers, which show a reduced EO response due to the relaxation of the poled EO chromophores after several days,[12] the EO response of (MDABCO)$NH_4I_3$ remains constant after storage in ambient conditions for more than 2 weeks (Figure 4a). In addition, the crystal structure remains unchanged up to

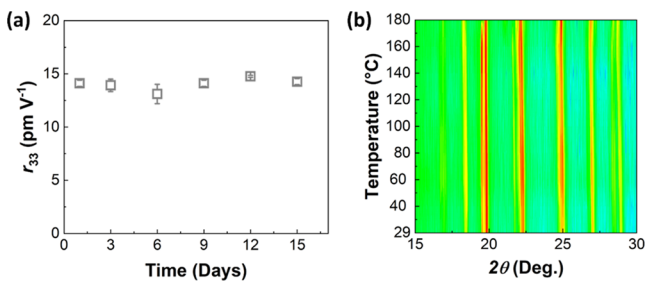


**Figure 4.** Stability. (a) Ambient-storage stability of the EO coefficient of the deficient (MDABCO)$NH_4I_3$ crystal. (b) Temperature-dependent powder XRD pattern of the deficient (MDABCO)$NH_4I_3$ crystal, showing stability up to 180 °C.

180 °C for 20 min (Figure 4b). The phase transition temperature—above which the crystal loses noncentrosymmetry and therefore second-order nonlinearity—of this perovskite is 170 °C (Supporting Information, Figure S5), similarly to that of the original crystals (173 °C),[16] higher than both the typical phase transition temperatures of organic EO polymers [e.g., 105 °C for poly(methyl methacrylate)] and the inorganic EO crystal barium titanate (BTO, 123 °C). We heated the crystals to 224 °C and did not see mass loss during the heating and cooling circle (Supporting Information, Figure S5). The improved thermal and storage stability of the (MDABCO)-


https://doi.org/10.1021/acsami.1c03406
ACS Appl. Mater. Interfaces XXXX, XXX, XXX–XXX

$NH_4I_3$ crystals highlight their suitability for use in on-chip EO modulation.

## 4. CONCLUSIONS

This work is the first demonstration, to our knowledge, of the linear EO response of metal-free halide perovskites, which can sustain toward high modulation frequency. When we introduced ammonium vacancies, we observed the linear EO of 14 pm $V^{-1}$, the highest measured among halide perovskites. The metal-free perovskite, which is both solution-processed and thermally stable, addresses challenges faced by organic and inorganic EO materials for integration on silicon photonics chips. This demonstration of EO in metal-free perovskites offers an additional route toward linear EO modulators for optical networks.

## ■ ASSOCIATED CONTENT

### Supporting Information

The Supporting Information is available free of charge at https://pubs.acs.org/doi/10.1021/acsami.1c03406.

Description of DFT calculation; additional figures of crystal characterizations (PDF)

## ■ AUTHOR INFORMATION


### Corresponding Author

**Edward H. Sargent** − *Department of Electrical and Computer Engineering, University of Toronto, Toronto, Ontario M5S 3G4, Canada;* orcid.org/0000-0003-0396-6495; Email: ted.sargent@utoronto.ca

### Authors

**Yuan Gao** − *Department of Electrical and Computer Engineering, University of Toronto, Toronto, Ontario M5S 3G4, Canada;* orcid.org/0000-0001-9407-1528

**Shadi Meshkat** − *Department of Physical and Environmental Sciences, University of Toronto Scarborough, Toronto, Ontario M1C 1A4, Canada*

**Andrew Johnston** − *Department of Electrical and Computer Engineering, University of Toronto, Toronto, Ontario M5S 3G4, Canada;* orcid.org/0000-0002-4545-532X

**Chao Zheng** − *Department of Electrical and Computer Engineering, University of Toronto, Toronto, Ontario M5S 3G4, Canada*

**Grant Walters** − *Department of Electrical and Computer Engineering, University of Toronto, Toronto, Ontario M5S 3G4, Canada;* orcid.org/0000-0002-9005-2335

**Qixin Feng** − *Department of Electrical and Computer Engineering, University of Toronto, Toronto, Ontario M5S 3G4, Canada;* orcid.org/0000-0003-1756-0090

**Xiaoping Wang** − *Neutron Scattering Division, Oak Ridge National Laboratory, Oak Ridge, Tennessee 37831, United States;* orcid.org/0000-0001-7143-8112

**Meng-Jia Sun** − *Department of Electrical and Computer Engineering, University of Toronto, Toronto, Ontario M5S 3G4, Canada;* orcid.org/0000-0001-8117-9257

**Amin Morteza Najarian** − *Department of Electrical and Computer Engineering, University of Toronto, Toronto, Ontario M5S 3G4, Canada;* orcid.org/0000-0002-0455-0451

**Dingjiang Xue** − *Department of Electrical and Computer Engineering, University of Toronto, Toronto, Ontario M5S 3G4, Canada;* orcid.org/0000-0002-7599-0008

**Ya-Kun Wang** − *Department of Electrical and Computer Engineering, University of Toronto, Toronto, Ontario M5S 3G4, Canada;* orcid.org/0000-0002-8970-6856

**Makhsud I. Saidaminov** − *Department of Electrical and Computer Engineering, University of Toronto, Toronto, Ontario M5S 3G4, Canada;* orcid.org/0000-0002-3850-666X

**Oleksandr Voznyy** − *Department of Physical and Environmental Sciences, University of Toronto Scarborough, Toronto, Ontario M1C 1A4, Canada;* orcid.org/0000-0002-8656-5074

**Sjoerd Hoogland** − *Department of Electrical and Computer Engineering, University of Toronto, Toronto, Ontario M5S 3G4, Canada;* orcid.org/0000-0002-3099-585X

Complete contact information is available at: https://pubs.acs.org/10.1021/acsami.1c03406


### Author Contributions

E.H.S. supervised the project. Y.G., D.X., and E.H.S. conceived the idea. Y.G. made the material and measured EO performance. S.M., G.W., C.Z., and O.V. did the DFT calculation. A.J. and X.W. conducted the neutron scattering measurement and did the analysis. Q.F. and M.J.S. contributed to the crystal growth and EO measurements. A.M.N. and Y.-K.W. carried out the powder X-ray diffraction measurement. Y.G. wrote the manuscript. A.J., M.I.S., S.H., and E.H.S. edited and revised the paper. All authors discussed the results and assisted during manuscript preparation.

### Notes

The authors declare no competing financial interest.

## ■ ACKNOWLEDGMENTS

This work was supported financially by the Natural Sciences and Engineering Research Council (NSERC) of Canada (950-231724). The single-crystal neutron diffraction experiment on TOPAZ beamline used resources at the Spallation Neutron Source, a DOE Office of Science User Facility operated by the Oak Ridge National Laboratory. The single-crystal analysis was performed at X-ray Crystallography Lab, University of Toronto. Computations were performed on the Niagara supercomputer at the SciNet HPC Consortium. SciNet was funded by: the Canada Foundation for Innovation; the Government of Ontario; Ontario Research Fund-Research Excellence; and the University of Toronto.

## ■ REFERENCES

(1) Wang, C.; Zhang, M.; Chen, X.; Bertrand, M.; Shams-Ansari, A.; Chandrasekhar, S.; Winzer, P.; Lončar, M. Integrated Lithium Niobate Electro-Optic Modulators Operating at Cmos-Compatible Voltages. *Nature* **2018**, *562*, 101−104.

(2) Reed, G. T.; Mashanovich, G.; Gardes, F. Y.; Thomson, D. J. Silicon Optical Modulators. *Nat. Photonics* **2010**, *4*, 518−526.

(3) Janner, D.; Tulli, D.; García-Granda, M.; Belmonte, M.; Pruneri, V. Micro-Structured Integrated Electro-Optic Linbo3 Modulators. *Laser Photonics Rev.* **2009**, *3*, 301−313.

(4) Poberaj, G.; Hu, H.; Sohler, W.; Günter, P. Lithium Niobate on Insulator (Lnoi) for Micro-Photonic Devices. *Laser Photonics Rev.* **2012**, *6*, 488−503.

(5) Wang, C.; Zhang, M.; Stern, B.; Lipson, M.; Lončar, M. Nanophotonic Lithium Niobate Electro-Optic Modulators. *Opt. Express* **2018**, *26*, 1547−1555.

(6) Wooten, E. L.; Kissa, K. M.; Yi-Yan, A.; Murphy, E. J.; Lafaw, D. A.; Hallemeier, P. F.; Maack, D.; Attanasio, D. V.; Fritz, D. J.; McBrien, G. J.; Bossi, D. E. A Review of Lithium Niobate Modulators

for Fiber-Optic Communications Systems. *IEEE J. Sel. Top. Quantum Electron.* **2000**, *6*, 69−82.
(7) Lee, M.; Katz, H. E.; Erben, C.; Gill, D. M.; Gopalan, P.; Heber, J. D.; McGee, D. J. Broadband Modulation of Light by Using an Electro-Optic Polymer. *Science* **2002**, *298*, 1401−1403.
(8) Shi, Y.; Zhang, C.; Zhang, H.; Bechtel, J. H.; Dalton, L. R.; Robinson, B. H.; Steier, W. H. Low (Sub-1-Volt) Halfwave Voltage Polymeric Electro-Optic Modulators Achieved by Controlling Chromophore Shape. *Science* **2000**, *288*, 119−122.
(9) Qiu, F.; Spring, A. M.; Maeda, D.; Ozawa, M.-a.; Odoi, K.; Otomo, A.; Aoki, I.; Yokoyama, S. A. Hybrid Electro-Optic Polymer and Tio 2 Double-Slot Waveguide Modulator. *Sci. Rep.* **2015**, *5*, No. 8561.
(10) Koeber, S.; Palmer, R.; Lauermann, M.; Heni, W.; Elder, D. L.; Korn, D.; Woessner, M.; Alloatti, L.; Koenig, S.; Schindler, P. C.; et al. Femtojoule Electro-Optic Modulation Using a Silicon−Organic Hybrid Device. *Light: Sci. Appl.* **2015**, *4*, e255.
(11) Alloatti, L.; Palmer, R.; Diebold, S.; Pahl, K. P.; Chen, B.; Dinu, R.; Fournier, M.; Fedeli, J.-M.; Zwick, T.; Freude, W.; et al. 100 Ghz Silicon−Organic Hybrid Modulator. *Light: Sci. Appl.* **2014**, *3*, e173.
(12) Marder, S. R.; Kippelen, B.; Jen, A. K.-Y.; Peyghambarian, N. Design and Synthesis of Chromophores and Polymers for Electro-Optic and Photorefractive Applications. *Nature* **1997**, *388*, 845−851.
(13) Dalton, L. R.; Harper, A. W.; Robinson, B. H. The Role of London Forces in Defining Noncentrosymmetric Order of High Dipole Moment−High Hyperpolarizability Chromophores in Electrically Poled Polymeric Thin Films. *Proc. Natl. Acad. Sci. U.S.A.* **1997**, *94*, 4842−4847.
(14) Wang, G.; Li, D.; Cheng, H.-C.; Li, Y.; Chen, C.-Y.; Yin, A.; Zhao, Z.; Lin, Z.; Wu, H.; He, Q.; Ding, M.; Liu, Y.; Huang, Y.; Duan, X. Wafer-Scale Growth of Large Arrays of Perovskite Microplate Crystals for Functional Electronics and Optoelectronics. *Sci. Adv.* **2015**, *1*, No. e1500613.
(15) Gao, Y.; Walters, G.; Qin, Y.; Chen, B.; Min, Y.; Seifitokaldani, A.; Sun, B.; Todorovic, P.; Saidaminov, M. I.; Lough, A.; Tongay, S.; Hoogland, S.; Sargent, E. H. Electro-Optic Modulation in Hybrid Metal Halide Perovskites. *Adv. Mater.* **2019**, *31*, No. 1808336.
(16) Ye, H.-Y.; Tang, Y.-Y.; Li, P.-F.; Liao, W.-Q.; Gao, J.-X.; Hua, X.-N.; Cai, H.; Shi, P.-P.; You, Y.-M.; Xiong, R.-G. Metal-Free Three-Dimensional Perovskite Ferroelectrics. *Science* **2018**, *361*, 151−155.
(17) Wang, F. Calculation of the Electro-Optical and Nonlinear Optical Coefficients of Ferroelectric Materials from Their Linear Properties. *Phys. Rev. B* **1999**, *59*, 9733.
(18) Coates, L.; Cao, H.; Chakoumakos, B.; Frontzek, M.; Hoffmann, C.; Kovalevsky, A.; Liu, Y.; Meilleur, F.; dos Santos, A.; Myles, D.; Wang, X.; Ye, F. A Suite-level Review of the Neutron Single-crystal Diffraction Instruments at Oak Ridge National Laboratory. *Rev. Sci. Instrum.* **2018**, *89*, No. 092802.
(19) Zikovsky, J.; Peterson, P. F.; Wang, X. P.; Frost, M.; Hoffmann, C. Crystalplan: An Experiment-Planning Tool for Crystallography. *J. Appl. Crystallogr.* **2011**, *44*, 418−423.
(20) Schultz, A. J.; Jørgensen, M. R. V.; Wang, X.; Mikkelson, R. L.; Mikkelson, D. J.; Lynch, V. E.; Peterson, P. F.; Green, M. L.; Hoffmann, C. M. Integration of Neutron Time-of-Flight Single-Crystal Bragg Peaks in Reciprocal Space. *J. Appl. Crystallogr.* **2014**, *47*, 915−921.
(21) Sheldrick, G. M. Crystal Structure Refinement with Shelxl. *Acta Crystallogr., Sect. C: Struct. Chem.* **2015**, *71*, 3−8.
(22) Yariv, A.; Yeh, P. *Photonics: Optical Electronics in Modern Communications*; Oxford University Press, 2007.
(23) Daly, J. C. *Fiber Optics*; Taylor & Francis, 1984; p 165.
(24) Li, G. L.; Yu, P. K. L. Optical Intensity Modulators for Digital and Analog Applications. *J. Lightwave Technol.* **2003**, *21*, 2010−2030.


https://doi.org/10.1021/acsami.1c03406
*ACS Appl. Mater. Interfaces* XXXX, XXX, XXX−XXX